Radio-frequency spectroscopy inside a laser cavity; "pure" nuclear quadrupole resonance of gaseous CH_3I

E. Arimondo,* P. Glorieux,† and Takeshi Oka
Herzberg Institute of Astrophysics, National Research Council of Canada, Ottawa, Ontario, Canada
(Received 2 December 1977)

The highly sensitive method of infrared-radio-frequency double resonance inside a laser cavity has been applied to the observations of "pure" nuclear quadrupole resonances of gaseous CH_3I corresponding to the transitions $\Delta J = 0$ and $\Delta F = \pm 1$. Radio-frequency signals with large signal-to-noise ratios ($\sim 10^4$) have been observed for many CO_2 and N_2O laser lines. The characteristic pattern of the radio-frequency spectrum specific to each rovibrational level has enabled us to assign the rotational levels, the infrared coincidences, and the associated far-infrared laser transitions unambiguously. From the radio-frequency spectrum the accurate vibrational and rotational dependences of the nuclear-quadrupole coupling constant and the values of the spin-rotation coupling constants have been determined. Because of the high sensitivity of the method, it was possible to observe collision-induced radio-frequency resonances as satellites to main line. This effect not only increases the number of observable quadrupole resonances, but also provides information on the detailed mechanism of rotational energy transfer. This method of observing "pure" quadrupole spectra of gases is applicable to any polar symmetric-top molecule with hyperfine structure which has rotational levels with double parity.

I. INTRODUCTION

The intensity of radio-frequency (rf) absorption spectrum is very small for two reasons: (i) the low energy of a photon $h\nu$, and (ii) the small population difference in thermal equilibrium of $h\nu/kT$. In molecular-beam resonance methods, one successfully avoids these points (a) by detecting molecules rather than radiation, and (b) by using state selectors to produce very nonthermal populational distribution. The infrared-rf double resonance in a laser cavity, used in the present paper,[1] avoids these points (i) by detecting infrared laser radiation rather than the rf radiation, and (ii) by producing a nonthermal distribution by infrared pumping.[2] The nonlinearity of the laser action further amplifies the signal. Thus we obtain a sensitivity which is several orders of magnitude greater than the straightforward absorption method. This highly sensitive method is now applied to observations of the rf nuclear quadrupole spectrum of gaseous CH_3I.

Nuclear quadrupole resonances are normally observed in solid-state samples in which a great number of nuclei give a few resonances.[3] An extension of this method to gases was first attempted by Sterzer and Beers[4] based on the idea that, although the density of nuclei is much less in gases than in a solid, the electric dipole moment rather than the nuclear magnetic moment is used as the transition moment. However, because of the two factors mentioned earlier, and because of the large partition functions of rotational levels, the observed signals were very weak in spite of the use of a long (6 m) rf cell and a long time constant of detection. Also the appearance of many lines corresponding to different rotational levels made the spectrum very dense. This method therefore has not been pursued further. The double-resonance method which we exploit here eliminates the last-mentioned difficulty because the laser singles out a pair of rotational levels associated with the pumping. A similar method which uses microwave-rf double resonance has been reported by Basov and Osipov[5] and by Osipov.[6] (See also a proposal by Shimoda.[7]) During the final preparation of this manuscript we also learned of the work by Sakai which is very similar to the work described in this paper. He observed "pure" nuclear quadrupole resonances of CH_3I, CD_3I, and CH_3Br.[8]

II. THEORY

A. Double resonance

The basic experimental set up to be analyzed is shown in Fig. 1. A coaxial rf cell containing CH_3I at a low pressure (~10 mTorr) is placed in an infrared laser cavity. The infrared laser line coincident with the molecular absorption is chosen by rotating a plane grating. For such a laser line

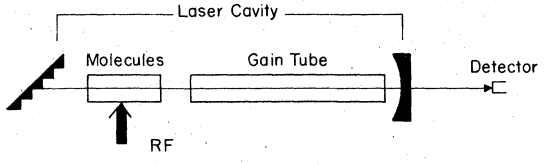

FIG. 1. Basic experimental setup for ir-rf double resonance inside the laser cavity.

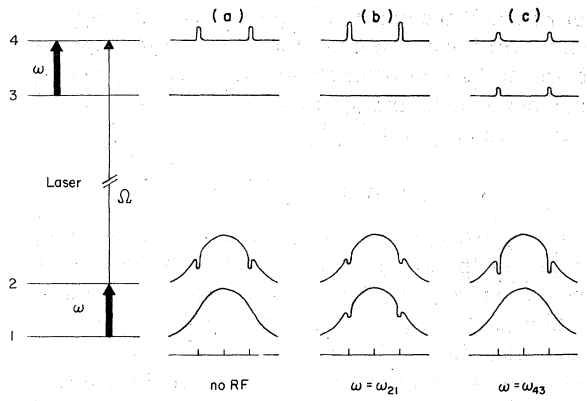

FIG. 2. Operation of infrared rf double resonance in saturated regime.

the CH_3I gas acts as a load. A powerful rf radiation (~ 5 W) is applied and its frequency is swept while the output laser power is monitored. When the rf frequency passes through a resonance, the load characteristics of the gas changes and a sharp variation of the laser output power is observed.

The response of molecules to the two radiations can be understood using the energy-population diagram shown in Fig. 2 [see also Ref. 2(b)]. The laser radiation with angular frequency Ω interacts with a group of molecules with a velocity component v which satisfies

$$\Omega_{\pm} \equiv \Omega(1 \pm v/c) = \Omega_0 \,. \tag{1}$$

Thus at a high-laser power and a low-gas pressure such as those used in our experiment, two symmetric "holes" are bleached in the Maxwellian velocity profile in the ground state and two "spikes" are produced in the excited state; this causes large nonthermal populational distributions between levels 1 and 2 and between 3 and 4 [Fig. 2(a)].

When the rf frequency ω is tuned to resonance in the ground state ω_{21} [Fig. 2(b)], it transfers molecules from the level 1 to 2 thus increasing the load characteristics of the gas. When the steady state is reached, the load for the laser is due to relaxation, i.e., the supply of molecules from other levels by collision. Such a supply is nearly doubled when the resonant rf radiation is present because the supply is made through two levels rather than one.

When ω is tuned to resonance in the excited state ω_{43} [Fig. 2(c)], the spikes produced in the level 4 are transferred to the level 3, again increasing the load characteristics of the gas because of the increased population difference for the infrared transition. When the steady state is reached, the load characteristics of the gas are larger because of the doubled channel for *drain* of pumped molecules. The double resonance occurring in the ground state and that in the excited state give signals that are very similar.

In the discussions given above, the infrared pumping of the $3 \leftarrow 1$ transition was neglected for simplicity. If $\omega_{21} \neq \omega_{43}$ but $|\omega_{21} - \omega_{43}| < \Delta\omega_D$, where $\Delta\omega_D$ represents the Doppler width for the infrared transitions, the laser interacts with two groups of molecules with different velocity components through the two infrared transitions $4 \leftarrow 2$ and $3 \leftarrow 1$. For this case we can use the same discussion as above except that now the two groups of molecules contribute to the signals. If, on the other hand, ω_{21} is equal to ω_{43} within the homogeneous broadening of the transition, the laser radiation bleaches holes in the levels 1 and 2 and produce spikes in 3 and 4 for molecules with the same velocity component; the rf radiation then does not change populations and no signal is obtained. This was demonstrated by experiments for high J parallel transitions where the hyperfine splittings are very similar in the ground and excited states.

B. Rate equations

In the qualitative discussions given above, we considered only variations in number of molecules and their effect through absorption, that is, coherence and dispersive effects were neglected. Within this approximation, the discussion can be made more quantitative by using rate equations. Similar treatments have been given by Takami[9] and Shimoda[2(a)] for infrared-microwave double resonance [see also Sec. 5 of Ref. 2(b)], and by Wormbecher, Harris, and Wicke[10] for optical-microwave double resonance.

The rate equation can be written

$$\dot{\vec{n}}(v) = \int_{-\infty}^{+\infty} \vec{K}(v, v') \cdot \vec{n}(v')dv' + \vec{R}(v) \cdot \vec{n}(v) \,, \tag{2}$$

where $\vec{n}(v)$ is a vector composed of $n_i(v)$ which are taken such that $n_i(v)dv$ represents the number of molecules in the ith level with a velocity component between v and $v+dv$. The collision matrix $\vec{K}(v, v')$ has off-diagonal matrix elements $k_{ij}(v')\rho_{ij}(v, v')$, which represents rates for the collision-induced transitions $i \leftarrow j$ with a velocity variation $v \leftarrow v'$, where $\rho_{ij}(v, v')$ is normalized by[11]

$$\int_{-\infty}^{+\infty} \rho_{ij}(v, v')dv = 1. \tag{3}$$

If we neglect velocity-changing elastic collisions, we obtain formally for diagonal elements

$$\rho_{ii}(v, v') = \delta(v, v') \,, \tag{4}$$

where $\delta(v, v')$ is Dirac's δ function, and

$$k_{ii}(v) = -\int_{-\infty}^{+\infty} \sum_j{}' k_{ji}(v)\rho_{ji}(v', v)dv'$$
$$= -\sum_j k_{ji}(v) \equiv -\gamma_i(v). \quad (5)$$

The radiative matrix $\tilde{R}(v)$ does not change v and for the situation shown in Fig. 2, has only four pairs of off-diagonal elements and four diagonal elements. The off-diagonal elements are

$$R_{ij}(v) = \frac{\gamma_{ij}|\mu_{ij}|^2}{2\hbar^2}\left(\frac{E_+^2}{(\Omega_+ - \omega_{ij})^2 + \gamma_{ij}^2} + \frac{E_-^2}{(\Omega_- - \omega_{ij})^2 + \gamma_{ij}^2}\right), \quad (6)$$

with $(i, j) = (3, 1)$ and $(4, 2)$ for the infrared transitions induced by the traveling wave laser fields E_+ and E_-, and

$$R_{ij} = \frac{\gamma_{ij}|\mu_{ij}|^2 E_r^2}{2\hbar^2[(\omega - \omega_{ij})^2 + \gamma_{ij}^2]}, \quad (7)$$

with $(i, j) = (2, 1)$ and $(4, 3)$ for the transitions induced by the rf field E_r. The diagonal elements are $R_{ii} = -\sum_j' R_{ij}$ with $i = 1$, 2, 3, and 4.

C. Thermal bath model

The steady-state molecular populations are obtained by solving Eq. (2) with $\dot{\tilde{n}}(v) = 0$. In order to express the solution in analytical form, however, a further simplifying assumption is needed. The simplest model which is almost always used (see, for example, Ref. 12) is the "thermal bath" model. In this model collisional transfer of the populational change induced by radiation to other levels is neglected. Mathematically, this amounts to equalizing the molecular population $n_i(v)$ which are not directly interacting with radiation to their equilibrium value $n_i^0(v)$ and neglect k_{12}, k_{13}, etc. compared with γ. By using Eqs. (3)–(5) and the principle of detailed balancing

$$k_{ij}(v')\rho_{ij}(v, v')n_j^0(v') = k_{ji}(v)\rho_{ji}(v', v)n_i^0(v), \quad (8)$$

we then have

$$\sum_j \int_{-\infty}^{+\infty} k_{ij}(v')\rho_{ij}(v, v')n_j(v')dv' = \gamma_i(v)[n_i^0(v) - n_i(v)]. \quad (9)$$

Thus we have for our system the rate equations

$$\begin{aligned}
\dot{n}_1 &= -\gamma_0(n_1 - n_1^0) + R_{21}(n_2 - n_1) + R_{31}(n_3 - n_1) = 0, \\
\dot{n}_2 &= -\gamma_0(n_2 - n_2^0) + R_{21}(n_1 - n_2) + R_{42}(n_4 - n_2) = 0, \\
\dot{n}_3 &= -\gamma_0 n_3 + R_{43}(n_4 - n_3) + R_{31}(n_1 - n_3) = 0, \\
\dot{n}_4 &= -\gamma_0 n_4 + R_{43}(n_3 - n_4) + R_{42}(n_2 - n_4) = 0.
\end{aligned} \quad (10)$$

In Eqs. (10) the velocity v is dropped from $n_i(v)$ and $\gamma_i(v)$ for simplicity, the equilibrium populations in the vibrationally excited states n_3^0 and n_4^0 are neglected, and γ_i ($i = 1$, 2, 3, and 4) are assumed to be equal to γ_0.

D. Molecular population

If $|\omega_{21} - \omega_{43}| = |\omega_{31} - \omega_{42}| \gg \mu_{ij}E/\hbar$, γ_0, we can consider the group of molecules with the velocity condition [Eq. (1)] for $\Omega_0 = \omega_{42}$ separately from the other for $\Omega_0 = \omega_{31}$. Solving the three steady-state equations for n_1, n_2, and n_4, with $R_{31} = R_{43} = 0$ we obtain the variation of the population difference $n_2 - n_4$ (which determines the laser operation) with and without the rf radiation ω_{21} as

$$\Delta[n_2(v) - n_4(v)] = \frac{\gamma_0}{1 + R_{42}(v)/\gamma_0} \frac{R_{21}/\Gamma_2}{1 + (1/\gamma_0 + 1/\Gamma_2)R_{21}} \times \left(\frac{n_1^0(v)}{\gamma_0} - \frac{n_2^0(v)}{\Gamma_2}\right), \quad (11)$$

where the effective relaxation rate

$$\Gamma_2 = \Gamma_4 \equiv \gamma_0\left(1 + \frac{R_{42}(v)}{\gamma_0 + R_{42}(v)}\right) \quad (12)$$

has been introduced. The last expression in Eq. (11) multiplied with γ_0 represents the population difference between levels 1 and 2 under infrared pumping. In order for this to be large, it is essential that Γ_2 is appreciably different from γ_0, that is, from Eq. (12), $R_{42}(v) \gtrsim \gamma_0$ (infrared saturation). However if the infrared radiation is too strong ($R_{42} \gg \gamma_0$) the first factor in Eq. (11) reduces the effect of rf resonance. For $n_1^0 \cong n_2^0$ the optimum value of $R_{42}(v)$ is $\simeq \gamma_0/\sqrt{3}$.[2(b)] Equation (11) also indicates that the rf saturation $R_{21} \gtrsim \Gamma_2$ is essential.

Similarly the variation of $n_2 - n_4$ by the rf resonance in the excited state ω_{43} can be obtained as

$$\Delta[n_2(v) - n_4(v)] = \frac{\gamma_0}{1 + R_{42}(v)/\gamma_0} \frac{R_{43}/\Gamma_2}{1 + (1/\gamma_0 + 1/\Gamma_2)R_{43}} \times \frac{R_{42}(v)}{\gamma_0 + R_{42}(v)} \frac{n_2^0(v)}{\Gamma_2}. \quad (13)$$

Since $R_{42}(v)/\Gamma_2[\gamma_0 + R_{42}(v)] = 1/\gamma_0 - 1/\Gamma_2$, Eqs. (11) and (13) are identical in the approximation $n_1^0(v) = n_2^0(v)$ and $R_{21} = R_{43}$; the rf resonance in the excited state and that in the ground state affect the laser operation in very similar ways and give almost identical signals.

If the difference between ω_{31} and ω_{42} is of the order of, or less than, the Doppler width $\Delta\nu_0$, the laser is also affected by $\Delta[n_1(v) - n_3(v)]$, which now has a maximum at a velocity v different from

that for the maximum of $\Delta[n_2(v)-n_4(v)]$. The value of $\Delta[n_1(v)-n_3(v)]$ for the ω_{21} resonance is determined to be

$$\Delta[n_1(v)-n_3(v)]=\frac{\gamma_0}{1+R_{31}(v)/\gamma_0}\,\frac{R_{21}\Gamma_1}{1+(1/\gamma_0+1/\Gamma_1)R_{21}}\times\left(\frac{n_2^0(v)}{\gamma_0}-\frac{n_1^0(v)}{\Gamma_1}\right), \tag{14}$$

which of course is identical with Eq. (11) except that (2, 4) and (1, 3) are interchanged.

Unlike in microwave-optical double resonance,[9,10] for which the difference between n_1^0 and n_2^0 is still sizable, in rf-optical double resonance n_1^0 and n_2^0 are very close and we have to rely almost solely on the difference between γ_0 and Γ_2 (or Γ_1) due to infrared saturation [see Eqs. (11) and (14)]. Therefore coincidence of the laser line with the molecular absorption within the Doppler profile is needed. The double resonance signals using off-resonant laser lines which are clearly observed in microwave-infrared double resonance[13,14] are very weak.

If $\omega_{31}=\omega_{42}$, both levels of the rf transition are strongly saturated for same velocity group of molecules and we have to rely on the difference between Γ_1 and Γ_2. Since for most cases $R_{31}\sim R_{42}$ for $\omega_{31}\sim\omega_{42}$, the signals in this case are very weak.

E. Bulk susceptibility

The variation of the bulk susceptibility of gas as an in-cavity load due to the rf switching is given by

$$\Delta\chi=\Delta\chi_{42}+\Delta\chi_{31}, \tag{15}$$

with

$$\Delta\chi_{ij}=-\frac{\mu_{ij}^2}{4\hbar}\int_{-\infty}^{+\infty}\left(\frac{1}{\Omega+kv-\omega_{ij}+i\gamma}+\frac{1}{\Omega-kv-\omega_{ij}+i\gamma}\right)\times\Delta[n_i(v)-n_j(v)]\,dv, \tag{16}$$

where it is assumed that $\gamma_{42}=\gamma_{31}\equiv\gamma$. This variation of bulk susceptibility of the gas affects the laser power. If we use the approximation $n_1^0(v)=n_2^0(v)$, $\Delta[n_i(v)-n_j(v)]$ is expressed as a product of Lorentzian functions by using Eqs. (6), (11), and (12). Therefore the integral in Eq. (16) can be performed by taking the Maxwellian distribution $n_1(v)$ out of the integral for the resonant velocity v_i which satisfies Eq. (1) and using contour integration. Thus for $|\Omega-\omega_{ij}|\gg\gamma$, we have for the ω_{21} resonance

$$\Delta\chi_{ij}(\omega)=\frac{i\pi}{4}\,\frac{c\mu_{ij}^2}{\Omega\hbar}\left(\frac{\mu_{ij}E}{\hbar}\right)^2\left(\frac{\gamma}{\gamma_0}\right)^2\phi(\gamma,\gamma',\gamma'')n_1^0(v_i)\times\frac{(\mu_{21}E_r/\hbar)^2}{(\omega-\omega_{21})^2+\gamma^2+(\gamma/\gamma_0)(\mu_{21}E_r/\hbar)^2}, \tag{17}$$

where v_i are resonant velocities satisfying Eq. (1) for $\Omega_0=\omega_{ij}$ and

$$\phi(\gamma,\gamma',\gamma'')=\frac{\gamma+\gamma'+\gamma''}{\gamma'\gamma''(\gamma+\gamma')(\gamma'+\gamma'')(\gamma''+\gamma)}, \tag{18}$$

with

$$\gamma'=\left[\gamma^2+\frac{\gamma}{\gamma_0}\left(\frac{\mu_{ij}E}{\hbar}\right)^2\right]^{1/2}$$

and

$$\gamma''=\left[\gamma^2+\frac{1}{2}\,\frac{\gamma}{\gamma_0}\,\frac{2\gamma_0+3R_{21}}{\gamma_0+2R_{21}}\left(\frac{\mu_{ij}E}{\hbar}\right)^2\right]^{1/2}.$$

Equation (17) indicates that, as expected from the qualitative discussions given in Sec. II A, (a) $\Delta\chi_{ij}(\omega)$ is purely dissipative, (b) only resonant molecules contribute to the signal, and (c) $\Delta\chi_{ij}(\omega)$ is Lorentzian except for a small dependence of γ'' on ω, in the approximation used in this treatment. If $|\Omega-\omega_{ij}|\lesssim\gamma$, saturation dip has to be considered and formulas (17) and (18) are slightly modified.

F. Collision-induced signals

The sensitivity of the rf spectrometer using a laser cavity is so high that signals are often observed on levels which are not directly pumped by the laser but are affected by collisional transfer of Bennett holes or spikes from the pumped levels. The energy-level scheme for this effect is shown in Fig. 3. The Bennett holes (or spikes) produced in the level 1 (or 3) by the laser pumping are

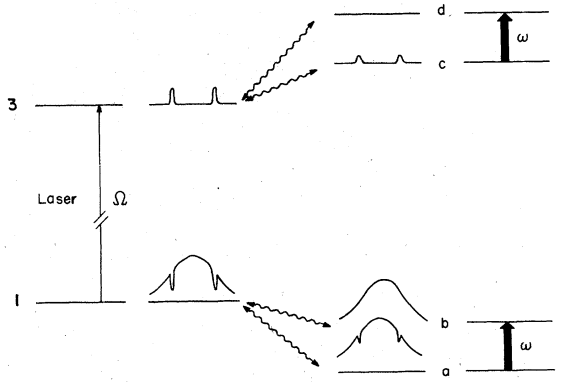

FIG. 3. Operation of double resonance on levels where a nonthermal population distribution is transferred by the collisions.

transferred by collisions to levels a and b (or c and d). Because of existence of selection rules for collision,[15] the efficiencies of the transfer from the level 1 to a and that from 1 to b are different and thus create a very nonthermal distribution between the levels a and b. When the resonant rf radiation is applied, the populations in the levels a and b are equalized and this effect is transferred by collision back to the level 1, thus affecting the laser output power.

In order to discuss the collision-induced rf signals using the rate equation [Eq. (2)], we have to extend the "thermal bath" model described in Sec. II C. We use the simplest extension in which the molecular populations of the four levels involved in the collisional and radiative transfer $n_1(v)$, $n_3(v)$, $n_a(v)$, and $n_b(v)$ are considered in detail but the populations of other levels are assumed to remain at their equilibrium value. By using

$$\int_{-\infty}^{+\infty} \vec{\vec{K}}(v, v')\,\vec{n}^0(v')\,dv' = 0 \tag{19}$$

for the equilibrium value $n_i^0(v')$, and considering $\delta n_i(v) \equiv n_i(v) - n_i^0(v)$, we obtain the following four steady-state equations:

$$\dot{n}_1(v) = \int_{-\infty}^{+\infty} [k_{1a}(v')\rho_{1a}(v, v')\delta n_a(v') + k_{1b}(v')\rho_{1b}(v, v')\delta n_b(v')]\,dv' - R_{31}(v)[n_1^0(v) + \delta n_1(v) - \delta n_3(v)] - \gamma_0 \delta n_1(v) = 0 ,$$

$$\dot{n}_3(v) = R_{31}(v)[n_1^0(v) + \delta n_1(v) - \delta n_3(v)] - \gamma_0 \delta n_3(v) = 0 , \tag{20}$$

$$\dot{n}_a(v') = \int_{-\infty}^{+\infty} [k_{a1}(v'')\rho_{a1}(v', v'')\delta n_1(v'') + k_{ab}(v'')\rho_{ab}(v', v'')\delta n_b(v'')]\,dv'' - R_{ba}[\delta n_a(v') - \delta n_b(v')] - \gamma_0 \delta n_a(v') = 0 ,$$

$$\dot{n}_b(v') = \int_{-\infty}^{+\infty} [k_{b1}(v'')\rho_{b1}(v', v'')n_1(v'') + k_{ba}(v'')\rho_{ba}(v', v'')\rho_{ba}(v'')]\,dv'' + R_{ba}[\delta n_a(v') - \delta n_b(v')] - \gamma_0 \delta n_b(v') = 0 ,$$

where $R_{21}(v)$ and R_{ba} represent the infrared and rf pumping given in Eqs. (6) and (7), respectively. In deriving Eq. (20) the approximations $n_a^0(v) = n_b^0(v)$, $n_2^0(v) = 0$, and $\gamma_1 = \gamma_3 = \gamma_a = \gamma_b = \gamma_0$ have been used. Since $\delta n_a(v)$ and $\delta n_b(v)$ are much smaller than $\delta n_1(v)$ and $\delta n_3(v)$, Eq. (20) can be solved by iteration. We first solve the first two equations neglecting $\delta n_a(v)$ and $\delta n_b(v)$ and obtain $\delta n_1(v)$ and $\delta n_3(v)$, which represent the Bennett holes and spikes, respectively. We then substitute the value of $\delta n_1(v)$ in the latter two equations and obtain $\delta n_a(v')$ and $\delta n_b(v')$, which represent the effect of collisional transfer of Bennett holes. From these expressions we can determine the variations of $\delta n_a(v')$ and $\delta n_b(v')$ by rf switching. These variations are then substituted to the first two equations to find $\Delta[n_1(v) - n_3(v)]$, which determines the variation of the laser power due to rf switching. We find

$$\Delta[n_1(v) - n_3(v)] = \frac{1}{\gamma_0 + 2R_{31}(v)} \frac{1}{\gamma_0 + k_{ab}} \frac{R_{ba}}{\gamma_0 + k_{ab} + 2R_{ba}} \times \int_{-\infty}^{+\infty} dv' \int_{-\infty}^{+\infty} dv''[k_{1a}(v') - k_{1b}(v')][k_{a1}(v'') - k_{b1}(v'')]\rho_{1a}(v, v')\rho_{a1}(v', v'') \frac{R_{31}(v'')}{\gamma_0 + 2R_{31}(v'')} n_1^0(v'') . \tag{21}$$

In deriving Eq. (21) we assumed $\rho_{1a}(v, v') = \rho_{1b}(v, v')$ and $\rho_{ab}(v, v') = \delta(v, v')$. The evaluation of the integral in Eq. (21) depends on the analytical form of $\rho_{1a}(v, v')$, which gives the variation of the velocity resulting from the collision-induced transitions $a \leftrightarrow 1$. Based on the experimental demonstrations that some collision-induced transitions occur without much change of velocity,[11, 16-19] we express

$$\rho_{1a}(v, v') = \zeta_{1a}\,\delta(v, v') + \rho'_{1a}(v, v') , \tag{22}$$

where ρ'_{1a} is a slowly varying function of v and v', and $\zeta_{1a} < 1$. We see that $\rho'_{1a}(v, v')$ does not contribute much to the integral in Eq. (21). Neglecting $\rho'_{1a}(v, v')$, we have

$$\Delta[n_1(v)-n_3(v)] = \left(\frac{\zeta_{1a}[k_{1a}(v)-k_{1b}(v)]}{\gamma_0+k_{ab}}\right)^2 \times \frac{R_{31}(v)}{[\gamma_0+2R_{31}(v)]^2} \times \frac{R_{ba}}{1+2R_{ba}/(\gamma_0+k_{ab})} n_1^0(v) . \quad (23)$$

A comparison of Eq. (23) with Eq. (14) indicates that, at resonance, the collision-induced signals are weaker than the direct three-level signals approximately by a factor of

$$\eta = \left(\frac{k_{1a}(v)-k_{1b}(v)}{\gamma_0+k_{ab}}\zeta_{1a}\right)^2 . \quad (24)$$

This supports the intuitive arguments at the beginning of this section that, in order to see collision-induced signals, we need (i) selective collisions, that is, $k_{1a} \neq k_{1b}$ and k_{1a} or k_{1b} is not much smaller than γ_0+k_{ab}, and (ii) velocity-conserving collisions which transfer the Bennett holes, that is, $\zeta_{1a} \simeq 1$. The factor η is similar to that for four-level microwave double resonance[15] except for the square of the expression in the bracket and the presence of ζ_{1a}. The square is needed because two steps of collisional transfer $1 \rightarrow a$ and $a \rightarrow 1$ are involved in making the collision-induced rf signals observable. This is essentially because the laser radiation is working as the pump as well as the monitor radiation. In the microwave double-resonance experiment the pump and monitor are entirely separate and only one step of collisional transfer is needed for a collision-induced signal.

Takami and Shimoda[9,20] have reported collision-induced double-resonance signals in an infrared-microwave double-resonance experiment on H_2CO. In their case, because of the sizable population difference for the microwave transition (at 48.285 GHz) and the weakness of the laser power, the signal was caused mainly by the one step process similar to microwave double-resonance experiments. The experimental evidence for the occurrence of two step processes in our work will be given in Sec. III.

Some of the collision-induced signals reported in this paper are caused by cascading collisional transfer of Bennett holes. For discussions of such effects we have to include more levels in the rate equation. More detailed discussion on such processes and elucidation of collisional properties of molecules will be given in a separate paper.

G. Intracavity arrangement

The variation of bulk gas susceptibility due to rf resonance such as that given in Eq. (17) is detected as a variation of the laser output power. Because of the intracavity arrangement and nonlinearity of laser oscillation, the effect is greatly amplified and increases the signal-to-noise ratio of the spectrum. This arrangement is similar to nuclear and electronic magnetic-resonance experiments except that the laser oscillator is required to saturate the molecular absorption. Just as in a magnetic-resonance experiment, the signal is amplified by the Q factor of the oscillating circuit. Even larger signal gains can be obtained if the laser is operated near threshold. In such a region the absorption as well as the dispersion of the gas become important. However the effect of dispersion tends to be decreased when an integration is made over the Doppler-velocity profile.

The detection of weak absorption by intracavity measurements has been investigated from both theoretical and experimental points of view.[21-23] We use here the simple approach based only on populational considerations given in Ref. 21. From the solution of the rate equations for the populations of an active medium in a single-mode laser, the number of photons g in the laser output is written as a function of the gain α and the loss η inside the laser cavity as

$$g = \gamma/B(\alpha/\eta - 1) , \quad (25)$$

where B is the Einstein coefficient for the laser-stimulated emission and γ is the relaxation rate. A more detailed expression can be derived from the semiclassical treatment of Holt,[22] but Eq. (25) suffices for the present discussion.

From Eq. (25) the enhancement factor ξ can be obtained as

$$\xi \equiv \lim_{\Delta\eta\rightarrow 0} \frac{\Delta g/g}{\Delta\eta/\eta} = (\alpha/\eta^2)(\alpha/\eta - 1)^{-1} , \quad (26)$$

which indicates an increase in the detection sensitivity for an intracavity setup in comparison with a single-pass measurement. Near threshold $\alpha \simeq \eta$ and we have

$$\xi = (1/\eta)(\alpha/\eta - 1)^{-1} . \quad (27)$$

This equation demonstrates our previous argument that the signal is enhanced by the Q factor of the cavity $(1/\eta)$ and the threshold character of the laser emission $[(\alpha/\eta - 1)^{-1}]$.

Because of the intracavity arrangement, and the double-resonance operation, the intensities of observed rf signals are complicated functions of conditions. Therefore care has to be taken in comparing relative intensities of the rf signals.

III. HYPERFINE SPLITTING

In the $CH_3{}^{127}I$ molecule a hyperfine splitting occurs because of the interaction of the iodine nu-

clear quadrupole moment and the gradient of the molecular electric field at the nucleus position. We use $\vec{I}$ for the iodine nucleus angular momentum ($I=\frac{5}{2}$); $\vec{J}$ and $\vec{K}$ for the rotational angular momentum and its projection along the molecular symmetry axis, respectively; and $\vec{F}=\vec{J}+\vec{I}$ for the total angular momentum. The nuclear quadrupole energy for the iodine nucleus on the axis of the symmetric top is[24]

$$W_Q(I,J,F)=eqQ\left(\frac{3K^2}{J(J+1)}-1\right)f(I,J,K)$$

$$+E_Q^{(2)}\frac{(eqQ)^2}{B}+E_Q^{(3)}\frac{(eqQ)^3}{B^2}\,, \qquad (28)$$

where eqQ is the quadrupole coupling constant, $f(I,J,K)$ is the Casimir function, and $E_Q^{(2)}$, $E_Q^{(3)}$ are the coefficients for the second- and third-order perturbation contributions arising from the off-diagonal quadrupole Hamiltonian matrix elements. Moreover, we have to consider the rotational dependence of the nuclear quadrupole coupling constant due to the centrifugal distortion of the molecule. This is composed of the normal rotational dependence of any physical quantity

$$eqQ(J,K)=eqQ_0+\chi_J J(J+1)+\chi_K K^2 \qquad (29)$$

and a distortion term which has to be included in the energy expression of

$$\delta W_Q=\chi_d\frac{K^2(4K^2-1)}{J(J+1)}f(I,J,K)\,. \qquad (30)$$

The latter is the term which was introduced by Hougen for explaining the quadrupole hyperfine splitting anomaly in NH_3.[25]

An additional term needed for the analysis of the hyperfine structure is due to the magnetic interaction between the iodine nucleus and molecular rotation which is

$$W_{\text{mag}}=\frac{1}{2}\left(C_N+(C_K-C_N)\frac{K^2}{J(J+1)}\right)$$

$$\times[F(F+1)-J(J+1)-I(I+1)]\,, \qquad (31)$$

where C_N is the principal value of the nuclear coupling along the symmetry axis and C_K the principal value normal to that axis. Magnetic interactions involving the hydrogen nuclei ($I_H=\frac{3}{2}$ or $\frac{1}{2}$) have not been observed in our experiment and they will not be included in the data analysis of the present investigation. The energy formulas given above are exactly the same as those used by Burie *et al.*[26] in the analysis of their molecular beam CH_3I spectrum.

The dipole selection rules $\Delta K=0$ and $+\nleftrightarrow-$ for rotational transitions in a symmetric top molecule allow transitions with $\Delta J=0$ and $\Delta F=1$ between the hyperfine levels of rotational states with $K\neq0$, because these states have a double parity. In Fig. 4 the quadrupole splitting in the lower and upper states of an infrared transition are schematically shown. Five rf transitions ($\alpha,\beta,\gamma,\delta,\epsilon$) are allowed in each state. Because the hyperfine splitting has a similar pattern in the lower and upper state, the infrared transitions with $\Delta F=\Delta J$ are close in frequency, spanning a frequency range comparable to the Doppler width of the methyl iodide vibrational transitions. Thus the laser line can often pump all these transitions, producing holes and spikes in the Doppler-velocity profile for each of them, and all the five resonances are observed in both states. The $\Delta F\neq\Delta J$ infrared transitions have a larger spread in frequency, and if the laser has a coincidence with one of them, not all hyperfine level are pumped inside the Doppler-velocity distribution of the molecules. As a consequence only a few rf resonances are observed, and that provides information on the laser coincidence with the molecular transition.

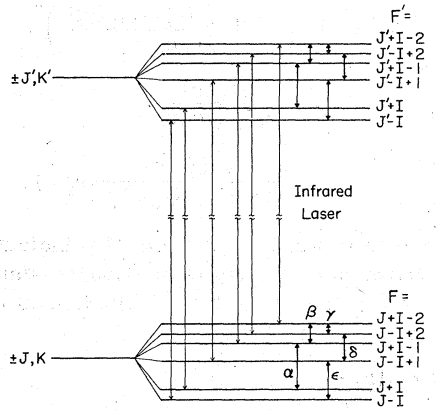

FIG. 4. Splitting of a set of vibration-rotation levels of CH_3I by the quadrupole interaction of the iodine nucleus.

IV. EXPERIMENTAL APPARATUS

The experimental setup, similar to that used in previous double-resonance experiments,[14,27] had the absorption cell containing CH_3I at a pressure between 2 and 40 m Torr inside the laser cavity. The cell, approximately 1 m long, was a coaxial 50-Ω transmission line terminated at one end with a dummy load. It was sealed with NaCl windows at the Brewster angle and placed inside the laser cavity near the grating. The rf radiation, amplitude modulated through an on-off switch, was amplified up to 10 W by an ENI 510L amplifier while the frequency was swept by a sawtooth voltage over the resonance values. The flowing gas CO_2 or N_2O

TABLE I. Hyperfine transition frequencies.

Laser line [a]		$^{12}CH_3I$ line		Perpendicular infrared transitions $\Delta K=+1$ (10 μm band) α	β	γ	δ	ϵ	α'	β'	γ'	δ'	ϵ'
$R16$	$^{12}CO_2$	$^rP(19,12)$	$\nu_6 \leftarrow 0$	···	16.175 [c]	4.726	22.194	···	···	59.340	16.175 [c]	79.312	···
$R2$	$^{12}CO_2$	$^rP(22,11)$	$\nu_6 \leftarrow 0$	86.156	36.995	···	45.376	78.736	20.596	9.170	···	10.346	18.764
$P4$	$^{12}CO_2$	$^rQ(11,9)$	$\nu_6 \leftarrow 0$	263.981	92.259	43.256	146.369	219.864	400.230	140.571	65.520	222.330	334.682
$P8$	$^{12}CO_2$	$^rR(9,8)$	$\nu_6 \leftarrow 0$	360.730	115.442	70.527	203.384	289.270	382.850	128.970	68.274	214.282	314.260
$P18$	$^{12}CO_2$	$^rR(44,5)$	$\nu_6 \leftarrow 0$	286.643	132.540	11.582 [c]	146.774	272.478	283.336	131.350	11.582 [c]	144.947	269.510
$P32$	$^{12}CO_2$	$^rR(15,5)$	$\nu_6 \leftarrow 0$	211.813	82.920	25.586	114.726	185.806 [c]	185.806 [c]	73.924	21.052	100.123	164.425
$P20$	$^{13}CO_2$	$^rR(6,1)$	$\nu_6 \leftarrow 0$	···	73.182	85.072	···	···	···	···	62.135	148.008	···
$P24$	$^{13}CO_2$	$^rQ(9,1)$	$\nu_6 \leftarrow 0$	···	···	···	173.550	247.219	···	···	53.691	156.104	···
$P24$	$^{13}CO_2$	$^rQ(10,1)$	$\nu_6 \leftarrow 0$	307.092	103.938	···	···	···	282.072	···	···	···	···
$R18$	N_2O	$^rR(8,8)$	$\nu_6 \leftarrow 0$	···	160.928	115.647	$\gamma+\delta=421.340$ [d]	···	···	···	105.870	306.708	···
$R12$	N_2O	$^rQ(17,8)$	$\nu_6 \leftarrow 0$	114.257	···	···	···	101.991	63.494	···	···	···	56.666
$R10$	N_2O	$^rP(50,11)$	$\nu_6 \leftarrow 0$	255.730	119.502	···	···	244.163	246.802	115.233	···	···	235.220
$P7$	N_2O	$^rQ(20,6)$	$\nu_6 \leftarrow 0$	···	···	20.900	120.183	···	···	···	···	105.504	179.744
$P25$	N_2O	$^rP(16,5)$	$\nu_6 \leftarrow 0$	222.428	···	···	120.024	196.596	170.088	···	···	92.034	149.295
$R34$	$^{12}CO_2$	$^rR(34,11)$	$\nu_3+\nu_6 \leftarrow \nu_3$	208.644	94.253	10.593 [c]	107.644	196.024	198.252	90.086	10.593 [c]	102.280	186.240
$P22$	$^{12}CO_2$	$^rQ(21,8)$	$\nu_3+\nu_6 \leftarrow \nu_3$	177.644	74.982	15.419	94.083	161.456	144.801	61.286	12.466	76.566	131.618
$P38$	$^{12}CO_2$	$^rR(18,5)$	$\nu_3+\nu_6 \leftarrow \nu_3$	238.776	97.638	···	120.740	213.556	218.748	90.830	···	116.760	197.072
$P42$	$^{12}CO_2$	$^rP(53,9)$	$\nu_3+\nu_6 \leftarrow \nu_3$	272.440	···	···	···	260.501	266.399	···	···	···	254.509
$R31$	N_2O	$^rR(24,9)$	$\nu_3+\nu_6 \leftarrow \nu_3$	···	77.776	13.386 [b]	94.798	···	···	71.394	12.524 [b]	85.728	···
$P8$	N_2O	$^rR(29,5)$	$\nu_3+\nu_6 \leftarrow \nu_3$	274.614	121.495	17.450	143.094	255.665	266.340	118.463	16.669	138.500	248.415
$R9$	N_2O	$^rR(20,2)$	$\nu_5 \leftarrow \nu_3$	295.572	123.243	27.268	157.245	267.126	281.250	118.452	25.052	148.896	255.420
$R6$	$^{12}CO_2$	$^rR(20,9)$	$2\nu_6 \leftarrow \nu_6$	128.836	53.984	11.551	68.431	116.713	107.536	45.635	9.199	56.868	97.724
$P16$	$^{12}CO_2$	$^rR(34,6)$	$2\nu_6 \leftarrow \nu_6$	273.090	123.170	14.835	141.312	256.547	266.178	120.514	14.017	137.481	250.316
$P34$	$^{12}CO_2$	$^rQ(20,6)$	$2\nu_6 \leftarrow \nu_6$	226.845	94.664	20.686	120.600	···	199.364	83.564	18.376	105.876	···
$P36$	$^{12}CO_2$	$^rR(9,5)$	$2\nu_6 \leftarrow \nu_6$	52.544	17.757	···	30.120	43.456	···	···	···	···	5.491
$P40$	$^{12}CO_2$	$^rP(24,6)$	$2\nu_6 \leftarrow \nu_6$	248.814	···	···	···	228.456	223.770	···	···	···	204.700
$P56$	$^{12}CO_2$	$^rR(7,3)$	$2\nu_6 \leftarrow \nu_6$	···	···	···	···	97.794	128.013	···	35.320 [b]	27.360	···
$R20$	N_2O	$^rR(15,8)$	$2\nu_6 \leftarrow \nu_6$	62.026	24.309	7.154	33.330	54.972	···	13.764	···	17.919	···
$P21$	N_2O	$^rQ(16,4)$	$2\nu_6 \leftarrow \nu_6$	253.800	100.935	···	137.136	224.115 [c]	224.115 [c]	89.505	···	120.648	197.704
$P48$	$^{12}CO_2$	$^rR(26,4)$	$2\nu_3+\nu_6 \leftarrow 2\nu_3$	···	122.391	···	147.450	···	···	119.301	···	142.620	···
$hP19$	$^{12}CO_2$	$^rQ(8,5)$	$2\nu_3+\nu_6 \leftarrow 2\nu_3$	14.265	···	···	···	10.029	161.884	···	···	···	125.175
$P13$	N_2O	$^rQ(21,7)$	$2\nu_3+\nu_6 \leftarrow 2\nu_3$	207.390	87.589	18.063	109.807	188.412	178.592	75.479	···	94.367	162.000
$P26$	$^{13}CO_2$	$^rR(9,2)$	$2\nu_3+\nu_6 \leftarrow 2\nu_3$	275.524	88.721	53.564	155.620	221.733	238.645	81.045	41.969	133.616	196.404
$P42$	$^{12}CO_2$	$^rQ(15,5)$	$\nu_2+\nu_6 \leftarrow \nu_2$	212.040	82.912	25.353	114.933	···	170.103	66.735	20.684	92.172	···
$P44$	$^{12}CO_2$	$^rR(9,4)$	$\nu_2+\nu_6 \leftarrow \nu_2$	148.095	48.219	28.756	83.978	119.940	100.707	34.755	17.600	56.604	···

TABLE I. (*Continued*)

Laser line	$^{13}CH_3I$ line		α	β	γ	δ	ϵ	α'	β'	γ'	δ'	ϵ'
Perpendicular infrared transitions $\Delta K = +1$ (10 μm band)												
$P26$	$^{12}CO_2$	$^rR(38,5)$	$\nu_6 \leftarrow 0$	283.545	129.100	...	146.128	267.848	278.950	127.800	...	143.586	263.774
$P29$	N_2O	$^rQ(8,4)$	$\nu_6 \leftarrow 0$	106.080	32.799	22.831	61.256	...	14.488	...	3.475	7.444	...
$P31$	N_2O	$^rR(12,3)$	$\nu_6 \leftarrow 0$	257.844	93.880	38.443	142.218	218.955	229.335	86.204	31.850	125.601	197.268
Parallel infrared transitions $\Delta K = 0$ (9.4 μm band)												
Laser line	$^{12}CH_3I$ line											
$9R16$	$^{12}CO_2$	$^qR(53,3)$	$2\nu_3 \leftarrow 0$	294.510[c]	138.222[c]	9.848	149.718[c]	281.748[c]	294.510[c]	138.222[c]	9.724	149.718[c]	281.748[c]
$9P34$	$^{12}CO_2$	$^qP(41,3)$	$2\nu_3 \leftarrow 0$	...	134.856	13.148	150.798[c]	278.196	...	134.550	13.416	150.798[c]	277.866
$9P4$	$^{12}CO_2$	$^qR(37,2)$	$3\nu_3 \leftarrow \nu_3$	...	134.840	14.572[c]	152.718[c]	279.505	...	135.032	14.572[c]	152.718[c]	279.725
$9P4$	$^{12}CO_2$	$^qR(38,5)$	$3\nu_3 \leftarrow \nu_3$	283.688	129.488	13.575[c]	146.153[c]	267.916	284.240	129.977	13.575[c]	146.153[c]	268.802
$9P6$	$^{12}CO_2$	$^qR(31,5)$	$3\nu_3 \leftarrow \nu_3$	277.446	123.825	16.492	144.192	259.224	278.634	124.764	16.092	144.474	...

[a] The CO_2 laser lines belong to the 00^01-$[10^00, 02^00]_I$ band (10.4 μm for $^{12}CO_2$ and 10.9 μm for $^{13}CO_2$) except those with $9P$ or $9R$ belonging to the 00^01-$[10^00, 02^00]_{II}$ (9.4 μm) band and that with hP belonging to the 01^11-$[11^10, 03^10]$ (10.8 μm) band.

[b] These frequencies have larger uncertainties and were not included in the least-squares fit.

[c] Unresolved doublets.

[d] Two-quantum rf transitions with $\Delta F = 2$.

laser, containing a 2.5-m gain cell, had a 5-m radius concave mirror at one end and a 10-μm blazed grating at the other. The output power of the laser was monitored by a Pb-Sn-Te detector, whose output was amplified, processed through a phase sensitive detector and registered on an X-Y recorder versus the scanning sawtooth voltage. In order to measure accurately the position of the resonance maximum, the detector output and the beating signal of the rf source with a stable rf oscillator were observed simultaneously on a dual-beam scope.

The precision of the frequency measurements depends on the possibility of locating the maximum of the resonance line with a reproducible accuracy. Thus an effort was made to reduce the resonance linewidth by operating at low-sample pressure and low-rf power. The accuracy depends also on the available signal-to-noise ratio; the precision attained in the measurements at 5 mTorr on resonance lines with a good signal-to-noise ratio was ~40 kHz. The limiting factors of the precision are saturation broadening and the ac Stark shift caused by the laser and by the rf radiation. This was unavoidable because of the double-resonance operation near the saturation regime, and because of the intracavity arrangement. Thus the present method increases the sensitivity greatly but not the precision. In order to do higher-resolution rf spectroscopy, it is necessary to place the cell outside the laser cavity, use much lower gas pressure to reduce pressure broadening, expand the laser beam to reduce the transit time broadening and reduce the laser and rf power. If all this is done the ultimate rf linewidth should be equal to the Doppler width corresponding to the rf frequency, that is ~1 kHz.

V. EXPERIMENTAL RESULTS

A. Double resonance

Double-resonance signals on the hyperfine structure of methyl iodide have been observed for infrared irradiation with the 10-μm bands of $^{12}CO_2$ and N_2O, the 9.4-μm band of $^{12}CO_2$ and the 10.9-μm band of $^{13}C^{16}O_2$. The laser lines for which quadrupole resonance has been observed and the rotational quantum numbers and the vibrational states have been definitively assigned are summarized in Table I.

The "pure" quadrupole resonances obtained with the 10-μm band lines of CO_2 and N_2O lasers have been thoroughly investigated and some typical spectra are presented in Figs. 5 and 6. From the measured positions of the $\Delta F = 1$ transitions between hyperfine levels of the lower and upper rovibrational states and from a rough estimate of

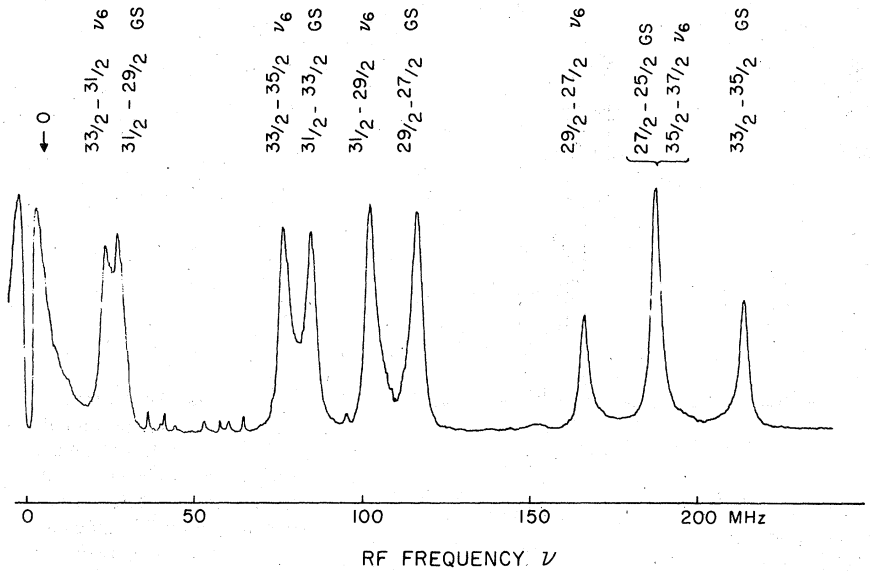

FIG. 5. An example of the observed resonances for CH_3I. A coincidence of the CO_2 $P(32)$ 10.72-μm line with the $\nu_6 \leftarrow 0$ $^rR(15,5)$ transition was used. Sample pressure ~10 mTorr. Note the pairs of quintets for the ground state and the excited state, very similar in shape.

the quadrupole coupling constant, the (J,K) rotational numbers of the states connected by the laser pump have been derived. The observed spectrum does not tell us which hfs transitions belong to the lower rovibrational state and which to the upper one. However, previous infrared investigations of vibrational spectra[28] in CH_3I show that laser lines in this spectral region excite perpendicular bands with $\Delta K = 1$. Based on this information the infrared transitions in Figs. 5 and 6 are identified, respectively, as $^rR(15,5)$ and $^rQ(11,9)$.

In the spectrum of Fig. 5 the ten hyperfine resonances have intensities of the same order of magnitude, proving that the laser pump is efficient for all the hyperfine levels. The spectrum of Fig. 6 shows strong signals on only four resonances and weak signals on all the remaining resonances. By looking at the hyperfine levels involved in the strong resonances we find that the laser line is near resonance only with the $F' = 19/2 \leftarrow F'' = 19/2$ transition, thus $\Delta F = \Delta J$ for this infrared rovibrational absorption. The intensities of the other double

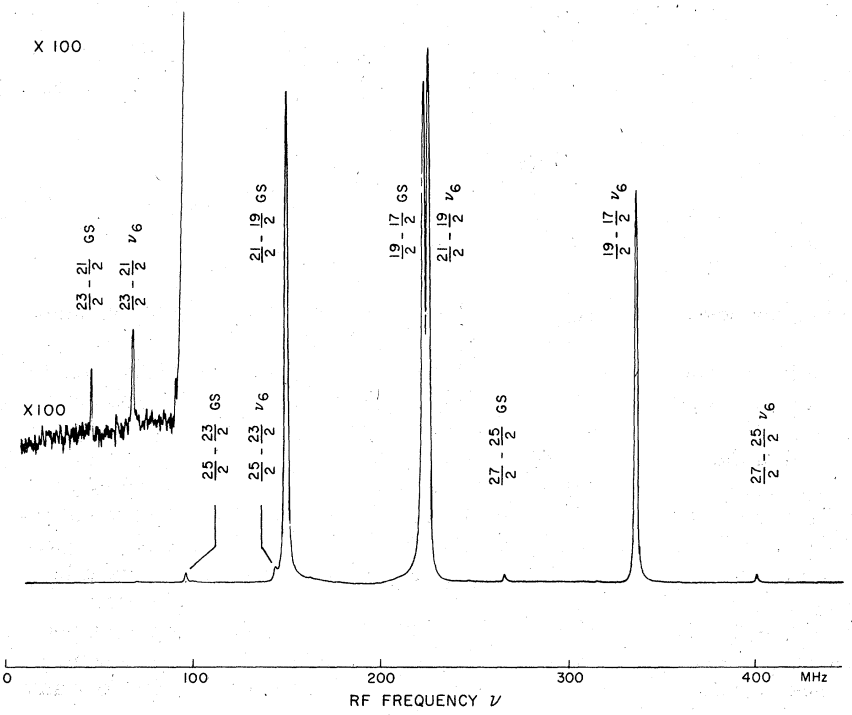

FIG. 6. An example of double resonance spectrum where strong resonances and weak signals were observed. For the second trace on the upper-left corner the sensitivity has been increased 100 times to record the double-resonance signals from the two remaining hyperfine transitions. A coincidence between the CO_2 $P(4)$ 10.44 μm line and $\nu_6 \leftarrow 0$ $^rQ(11,9)$ transition of CH_3I was used. Pressure ~8 mtorr. Time constant of detection ~30 msec.

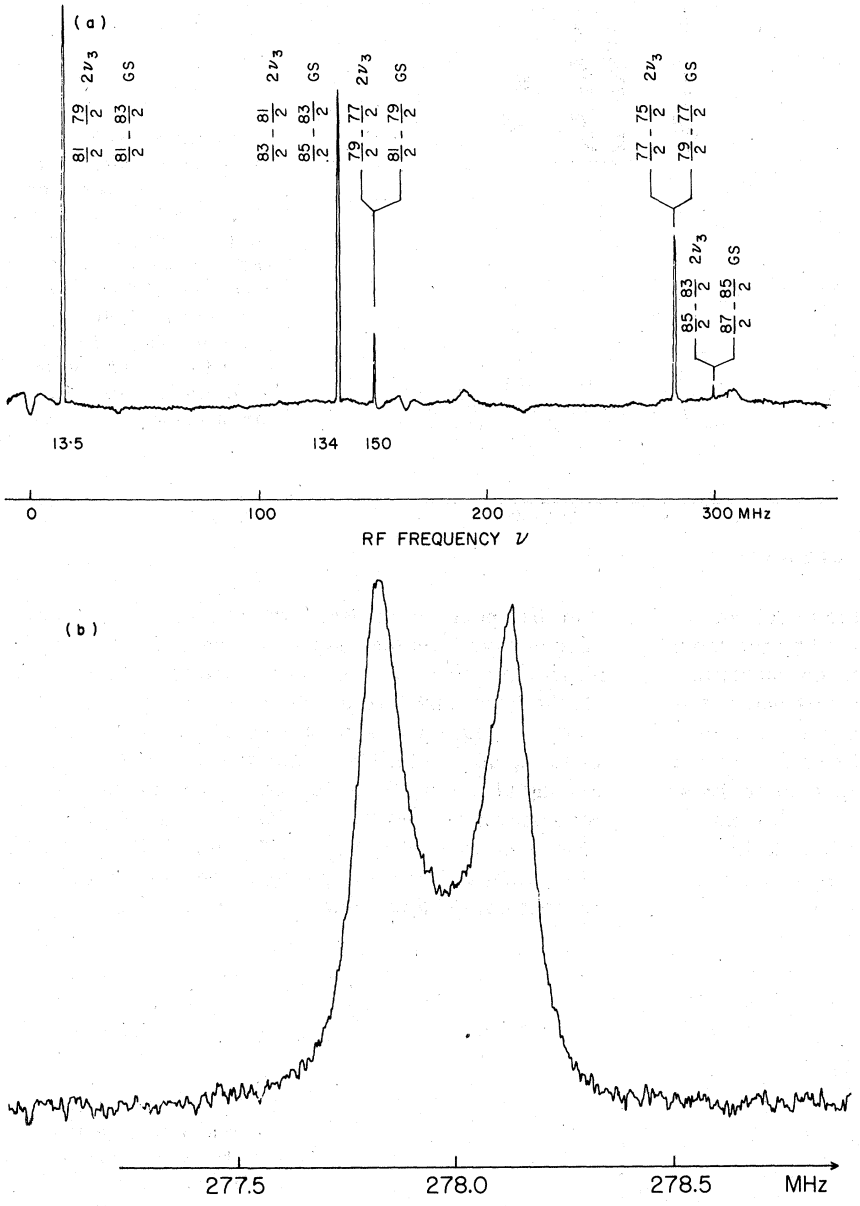

FIG. 7. (a) An example of double resonance signals for high J rotational levels in a parallel infrared band of CH_3I. The excited-state resonance and the ground-state resonance appear very close. A coincidence between the CO_2 $P(34)$ 9.68-μm line and the $2\nu_3 \leftarrow 0$ ^qP (41, 3) transition was used. Pressure ~5 mTorr. (b) Recording with an expanded frequency scale for a doublet of excited- and ground-state resonances. Pressure ~2 mTorr. Time constant of detection 30 msec.

resonances are explained by comparing the position of the infrared absorptions lines to the Doppler linewidth. The nearest transition is that connecting the $F' = \frac{25}{2}$ to the $F'' = \frac{25}{2}$ level and is shifted in frequency by +52 MHz. Because the half width at half maximum (HWHM) Doppler width of the infrared lines of CH_3I is ~26 MHz, the few molecules in the far wing of the Doppler profile can absorb infrared radiation for the $F' = \frac{25}{2} \leftarrow F'' = \frac{25}{2}$ transition. The $F' = \frac{21}{2} \leftarrow F'' = \frac{21}{2}$ transition has a Doppler shift of +76 MHz and this explains the low intensity of the rf transitions $F' = \frac{21}{2} \leftrightarrow F'' = \frac{23}{2}$ in both rovibrational states. However the intensities of the observed double-resonance signals are larger than expected on the basis of the number of molecules involved in the infrared transitions. This is partly due to the collisional effect discussed later. By tuning the laser frequency inside the laser-gain profile it is possible to change the relative intensity of the observed rf lines.

The double-resonance spectra observed by irradiation with the 9.4-μm band of CO_2 have coincidences with infrared absorption in the $2\nu_3 \leftarrow 0$ parallel band.[29] The typical spectrum, reported in Fig. 7(a), presents five pairs of very closely spaced doublets that disappear at a sample pressure larger than 10 mTorr. These components of a doublet are separated by about 100–500 kHz and

resolved under higher resolution as shown in Fig. 7(b). The infrared transitions investigated in this region have $\Delta J=\pm 1$, $\Delta K=0$, and $J=30-50$. The quadrupole coupling constant differs only slightly between the ground and ν_3 vibrational states, and the quadrupole splitting depends very little on J at large J numbers. As the pressure is increased the homogeneous broadening of the infrared transitions occurs and a double-resonance four-level scheme (Fig. 1) with $\Omega_{13}\simeq\Omega_{24}$ and $\omega_{12}\simeq\omega_{34}$ is realized. Because of the destructive interference phenomenon previously described the rf radiation does not change populations and no double-resonance signal is obtained. For the $\Delta J=0$ and $\Delta K=0$ transitions in the $2\nu_3-0$ band, because of the small change in the quadrupole coupling constant with the ν_3 vibration, this destructive interference phenomenon is always present and hyperfine double-resonance signals are not observed.

In the spectra of Figs. 5–7 a signal is observed when the rf field is swept over the zero-frequency value. The line shape of the observed signal is deformed by the low-frequency cutoff of the rf amplifier. The modification of the infrared absorption by the rf electric field produces this signal.

The zero-frequency double-resonance absorption indicates a near coincidence of the laser with an infrared transition in a molecule with double-parity levels, as can be derived from the double-resonance theoretical treatment of Ref. 2b.

B. Two-photon transitions

At high rf power, double-resonance spectra include transitions involving the simultaneous absorption of two quanta of the electromagnetic field, either an infrared and a rf quanta or those involving two rf quanta. In both cases a three-level scheme is required and the energies of the absorbed photons are algebraically added to match the energy separation between initial and final levels. An intermediate virtual level lies near a real one and the transition probability of the whole process depends inversely on the energy mismatch ΔE between the virtual and real levels.

The ir-rf two-photon processes occur when laser and rf frequencies satisfy the relation

$$\Omega_{\pm}+\omega=\Omega_0+\omega_0\,. \tag{32}$$

Such a transition can occur for instance between the levels 1 and 4 of Fig. 2. In a double-resonance spectrum where the rf field frequency is swept, these transitions appear with the width of the Doppler broadening, because of the thermal distribution of the molecular velocity appearing in Eq. (32). The center of the absorption depends upon

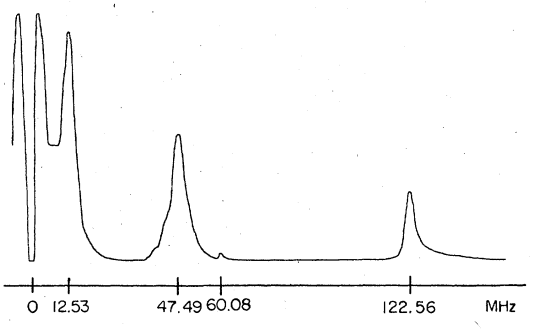

FIG. 8. Double-resonance spectrum observed for the coincidence between the $^{13}CO_2$ $P(36)$ 11.33-μm laser line and a ^pP (4, 3) transition of CH_3I. The resonance line at 60.08 MHz is a two-photon transition between the $F'=\frac{5}{2}\leftarrow\rightarrow F''=\frac{9}{2}$ hyperfine levels of the ($J=4$, $K=3$) rotational state.

the position of the laser frequency with respect to the molecular transition. In the spectrum of Fig. 5 a double-quantum ir-rf process is observed near 150 MHz, while in Fig. 6 the broad pedestals below the strong resonances are two-photon transitions of this type.

The rf two-quantum processes are $F\rightarrow F\pm 2$ transitions in the hyperfine levels of a rotational state and involve in the intermediate step a virtual level quasiresonant with the $F\pm 1$ hyperfine level. These transitions have a radiative rate $(\mu_{ij}E_r/\Delta E)^2$ smaller than that of a single-quantum transition [Eq. (7)], ΔE being the energy mismatch between the virtual level and the real one. These transitions appear as narrow resonances in the double-resonance spectrum. An example is shown in the spectrum of Figure 8 for the hyperfine transitions in a $(J=4,K=3)$ rotational level. The transition at 60.08 MHz is a rf two-quantum transition. In this case, where not all the hyperfine transitions are observed, the rf two-quantum transitions provide information on states not directly pumped by the laser radiation.

C. Collision-induced transitions

Several recordings show, beside the main resonances in the states $(J',K')-(J'',K'')$ pumped by the laser radiation, other resonances with a smaller intensity and distributed in the frequency range over both sides of the principal resonances. An example is shown in Fig. 9 for the higher-frequency hyperfine transitions in the $(\nu_6,J'=15,K'=6)$ and $(0,J''=16,K''=5)$ states. From an analysis of the resonance frequencies we have been able to identify these transitions as connected to states $(J'\pm n,K')$ and $(J''\pm m,K'')$, where through collisional processes the nonthermal distribution created by the laser pumping is transferred. The collisional processes involved in all the observed

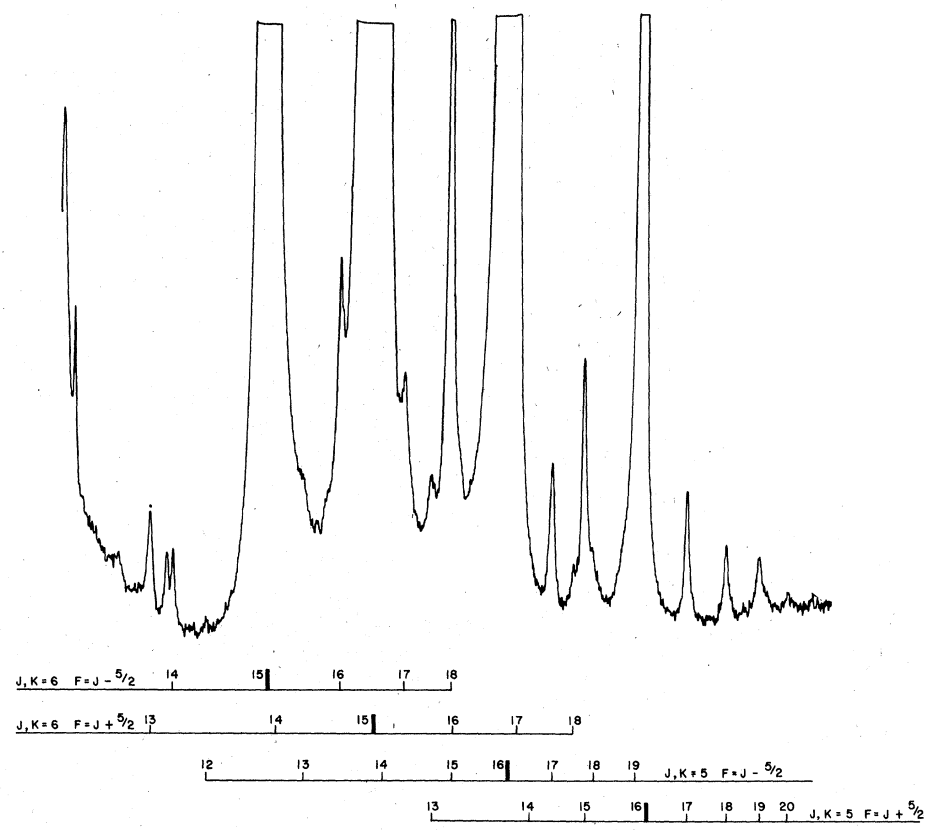

FIG. 9. An example of traces showing collision-induced quadrupole resonances. The normal resonance associated with directly pumped levels are off scale. The many smaller signals which appear as satellites to the main lines are collision-induced signals. A coincidence between N_2O $P(25)$ 10.90-μm line and the $\nu_0 \leftarrow 0$ $^rP(16,5)$ line of CH_3I was used. Sample pressure was 20 mTorr.

double-resonance signals satisfy the selection rule $\Delta K = 0$ valid for dipole-type collision in axially symmetric molecules.[15] All the collision processes that we have observed obey the selection rule $\Delta F = \Delta J$. If we suppose that during the collision the iodine nucleus is not perturbed, any change in the F quantum number is connected to a change in the J rotational number. Thus the transitions with $\Delta F = \Delta J$ have the largest transition probability for collisional transitions, as for radiative transitions. This behavior was observed earlier by Cohen and Wilson[30] using microwave double resonance and has also been applied to interpret the results of ir-microwave multiple-resonance experiments on ammonia.[31]

The collisional transfers occur between the (J,K,F) level and the $(J+n,K,F+n)$ level. This is evident from the double-resonances spectrum of Fig. 9, where the levels with $F=J+\frac{5}{2}$ and $F=J-\frac{5}{2}$ are pumped by the laser in both lower and upper rovibrational states. The same levels in other rotational states have a nonthermal population distribution because of the collisions and produce double-resonance signals.

The fact that the collision-induced signals are produced by two-step collision rather than one step, as discussed in Sec. II F, is obvious because if the latter was the case, the collision-induced signals in the excited state would be much weaker.

Collision-induced transitions have been useful to identify the quantum numbers of the rovibrational transitions pumped by the laser. The frequencies of the measured collision-induced hyperfine resonances are summarized in Table II and have been included in the data fit for deriving the hyperfine constants.

D. Hot bands

The high sensitivity of the method enabled us to observe not only the signals associated with the fundamental band $\nu_6 \leftarrow 0$ and the overtone band $2\nu_3 \leftarrow 0$ starting from the ground state but also other signals associated with hot bands. The infrared transitions which have been assigned are summarized in Fig. 10. It is interesting that the in-

TABLE II. Frequencies for collision-induced hyperfine resonances in $^{12}CH_3I$ (in MHz).

Laser line		State [a]	α	ϵ	Others
$R2$	$^{12}CO_2$	(0,21,11)	64.660	59.926	$\beta = 28.387$
$R2$	$^{12}CO_2$	(0,23,11)	104.334	95.530	$\delta = 54.900$
$P32$	$^{12}CO_2$	(0,13,5)	···	157.150	
$P32$	$^{12}CO_2$	(0,14,5)	198.700	172.700	
$P32$	$^{12}CO_2$	(0,16,5)	222.400	196.500	
$P32$	$^{12}CO_2$	(ν_6,14,6)	···	150.600	
$P32$	$^{12}CO_2$	(ν_6,15,6)	170.075	149.250	
$P32$	$^{12}CO_2$	(ν_6,17,6)	···	177.100	
$R12$	N_2O	(0,16,8)	90.430	80.080 [b]	
$R12$	N_2O	(0,18,8)	134.145	120.312	
$R12$	N_2O	(0,19,8)	···	136.000	
$R12$	N_2O	(ν_6,16,9)	33.050	29.522	
$P25$	N_2O	(0,15,5)	212.145 [b]	186.012 [b]	
$P25$	N_2O	(0,17,5)	231.373	205.835	
$P25$	N_2O	(ν_6,13,6)	127.209 [b]	109.131	
$P25$	N_2O	(ν_6,14,6)	150.600	131.295	
$P25$	N_2O	(ν_6,16,6)	···	164.708	
$P40$	$^{12}CO_2$	(ν_6,25,6)	···	232.608	
$P22$	$^{12}CO_2$	(ν_3,22,8)	188.560	···	$\delta = 99.603$
$P22$	$^{12}CO_2$	($\nu_3+\nu_6$,22,9)	···	···	$\delta = 83.535$
$P22$	$^{12}CO_2$	($\nu_3+\nu_6$,23,9)	···	···	$\delta = 89.868$
$P38$	$^{12}CO_2$	(ν_3,17,5)	231.228	205.476 [b]	
$P38$	$^{12}CO_2$	($\nu_3+\nu_6$,18,6)	209.904	187.792	
$P38$	$^{12}CO_2$	($\nu_3+\nu_6$,20,6)	226.656	···	

[a] The notation (ν_i,J,K) defines the vibrational and rotational assignment of the state.
[b] These frequencies have larger uncertainties and were not included in the least-squares fit.

tensities of the double-resonance signals associated with the hot-band transitions are much stronger than expected from the Boltzmann factors of the lower states of hot bands which are about $\frac{1}{10}$, $\frac{1}{100}$, $\frac{1}{100}$, and $\frac{1}{1000}$ for the ν_3(533.2 cm^{-1}), ν_6(882.7 cm^{-1}), $2\nu_3$(1059.9 cm^{-1}), and ν_2(1250.8 cm^{-1}) state, respectively. We think this is partly because of the heating of the gas by the laser and partly because of the nonlinearity of the sensitivity with respect to the number of molecules. Many resonances which have not been assigned may be associated with even higher hot-band transitions.

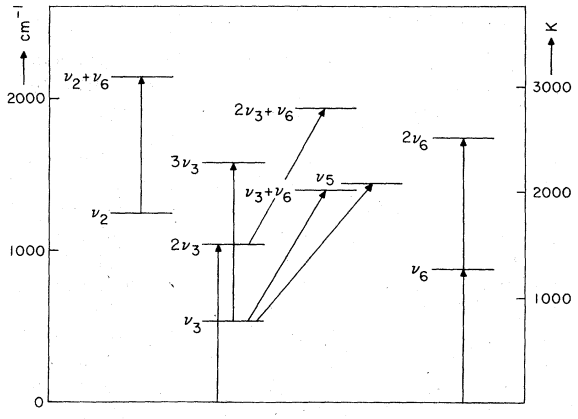

FIG. 10. Vibrational energy levels and transitions studied.

VI. ANALYSIS

A. Rovibrational assignment

The rotational quantum numbers of the observed double-resonance signals have been assigned by using their resonance patterns. Because the pattern is characteristic of each J and F, it was often possible for lower rotational levels to assign these quantum numbers even if the quadrupole coupling constant is not precisely known. The value of K was then assigned from the spread of the pattern. For higher levels, the resonance pattern does not depend on quantum numbers as much (a variation of a few parts in thousand is observed when J is increased by one) and the assignment needed the value of eqQ with a medium accuracy.

The vibrational assignment was done by using the results of previous infrared investigations which gave approximate information on the laser coincidences. The results of Ref. 28 ($\nu_6 \leftarrow 0$, $\nu_2+\nu_6 \leftarrow 0$), Ref. 29 ($2\nu_3 \leftarrow 0$), and Ref. 32 ($\nu_3+\nu_6 \leftarrow 0$, $\nu_5 \leftarrow 0$, $\nu_2 \leftarrow 0$) proved useful. For other states such as

$2\nu_6$, $3\nu_3$, and $2\nu_3+\nu_6$ which have never been studied, we used extrapolation from lower states. The vibrational dependence of the quadrupole coupling which is later listed in Table IV was also used for the vibrational assignment. This was particularly useful for assigning vibrations with ν_6 and $2\nu_6$ because this vibrational mode showed large variation of eqQ. For an initial guess, the vibrational dependence of eqQ reported by Hirose and co-workers[33] was useful.

Some double-resonance signals observed in the 10.4-μm region have been identified as due to $^{13}CH_3I$ in natural abundance, based on the infrared work by Duncan and Allan.[34] These assignments were confirmed by using a 10% ^{13}C enriched sample.

Based on the recipe given above and by using the computer programs of Burie *et al.*, the assignment and analysis proceeded as follows. About one third of the double-resonance signals observed in the 10.4-μm region were easily assigned as due to the ν_6-0 transitions of $^{12}CH_3I$. The calculated infrared frequencies based on the constants of Matsumura and Overend[28] agreed well with laser lines within the uncertainty. From the analysis of these resonances using the parameters of Burie *et al.* for the ground state,[26] we obtained accurate hyperfine constants for the ν_6 state. During this process we also improved the value of χ_d over that reported earlier.[26] We then calculated the values of eqQ for each resonance pattern by using other constants fixed at the ground-state values or at ν_6 state. The assignment of the $2\nu_6-\nu_6$ was done by observing (i) very good agreement of the pattern in one state with the calculated values using ν_6 constants, and (ii) the rather large variation of eqQ (−12.4 MHz) from the ground state.

For the ν_2, ν_3, and ν_5 excitation, the variation of eqQ was not so large and the assignment of the $\nu_3+\nu_6-\nu_3$, $\nu_2+\nu_6-\nu_2$, and $\nu_5-\nu_3$ was done with calculated frequencies using the results of previous work.[28,32] The $\nu_5-\nu_3$ transition gains intensity because of the Fermi interaction between $\nu_6+\nu_3$ and ν_5.[32] The group of resonances which have eqQ very close to that of the ground-state and infrared frequencies shifted by −14 cm^{-1} from the ν_6-0 transitions were assigned to $2\nu_3+\nu_6-2\nu_3$. The anharmonicity shift observed in $\nu_3+\nu_6$ and $2\nu_3$ could give extrapolated value for the $2\nu_3+\nu_6$ level which agrees with the observed shift.

In the 9.4-μm region, most transitions were assigned to the $2\nu_3-0$ transitions on the basis of previous infrared work.[29] The remaining transitions have been identified as $3\nu_3-\nu_3$ giving the frequency shifts expected from the extrapolation.

Although we could assign most of the observed lines, some transitions were left unassigned. The double-resonance spectrum shown in Fig. 8 is an example. The rotational assignment for this pattern is definite and the infrared transition must be $^pP(4,3)$. The value of eqQ for the lower state is −1933.3 ± 1.0 MHz. The resonances for the upper state are observed at 1.33, 2.54, and 3.08 MHz. However its vibrational assignment is not known.

B. Hyperfine constants

The "pure" quadrupole resonances measured and assigned are presented in Table I, and the collision-induced transitions in Table II. A least-squares fit has been applied to derive the quadrupole and spin-rotation interaction constants. The measurements have been weighted on the basis of the signal to noise obtained in the double-resonance spectrum. For the ground-state fit the eqQ constant has been fixed at the very accurate value derived in the molecular-beam experiments.[26,36] The ground-state quadrupole centrifugal corrections and the spin-rotation constants resulting from the fit of hyperfine transitions measured in the present paper together with Osipov's rf-microwave double-resonance measurements[6] are shown in Table III. The precision is higher than that obtained in the molecular-beam experiment,[26] because of the large number of measured hyperfine transitions. Moreover, states with K number up to 11 have been observed so that the correlation factor between the χ_K and χ_d constants is only 0.7 as compared to the 0.998 obtained in the molecular-beam experiment. The standard deviation of the least-squares fit was 54 kHz. The hyperfine frequencies in the states with $K=J\simeq 10$ have a deviation systematically larger than all the other measurements; this behavior is due to the infrared and rf ac Stark effects larger in these states than in others. The analysis of resonances in the ν_6 state has produced the six hyperfine constants as shown in Table III.

TABLE III. Quadrupole coupling constants, spin rotation constants, and rotational dependence of quadrupole coupling constants for 0 and ν_6 vibrational states of $^{12}CH_3I$.

	Ground state	ν_6 state
eqQ (MHz)	−1934.136[a]	−1940.50(60)
C_N (KHz)	17.6(10)	17.3(21)
C_K (KHz)	17.0(46)	29.9(69)
χ_J (KHz)	−1.63(22)	−1.32(64)
χ_K (KHz)	−38.2(61)	−44(12)
χ_d	22.9(23)	23.5(34)

[a] Fixed at the value of Ref. 36. The uncertainties shown in parentheses in units of the last digit are three times the standard deviations.

TABLE IV. Vibrational dependence of quadrupole coupling constant.

		eqQ (MHz)	3σ (MHz)	Δ (obs − calc)	Ref.
$^{12}CH_3I$	Ground state	−1934.136	0.015	···	36
	ν_3	−1934.52	0.34	0.22	
	ν_6	−1940.50	0.60	0.10	
	$2\nu_3$	−1934.80	0.61	0.33	
	ν_2	−1936.37	1.84	−0.32	
	$\nu_3+\nu_6$	−1940.57	0.87	−0.02	
	ν_5	−1934.5	3.0	···	33(b)
	$3\nu_3$	−1934.48	0.39	−0.16	
	$2\nu_6$	−1946.59	1.14	−0.11	
	$2\nu_3+\nu_6$	−1940.32	1.44	−0.44	
	$\nu_2+\nu_6$	−1944.64	4.32	+1.67	
	ν_1	−1937.06	0.09	···	35
$^{13}CH_3I$	Ground state	−1934.12	0.80	···	
	ν_6	−1941.06	0.69	···	
		δ (MHz)	3σ (MHz)		
$^{12}CH_3I$	$\delta(eqQ)_1$	−2.92	0.09		35
	$\delta(eqQ)_2$	−2.55	1.69		
	$\delta(eqQ)_3$	−0.17	0.14		
	$\delta(eqQ)_5$	−0.4	3.0		
	$\delta(eqQ)_6$	−6.28	0.48		

For the remaining vibrational states less data were available. Thus only the quadrupole coupling constant has been derived from the fit, all the other constants being fixed to the average of the ground and ν_6 results. The quadrupole coupling constants measured in this experiment and in the remaining vibrational states in other previous investigations have been collected in Table IV.

The eqQ dependence on the vibrational state can be expressed as

$$eqQ_{\Sigma v_i} = eqQ_0 + \sum_i \delta(eqQ)_i v_i . \tag{33}$$

A least-squares fit of this vibrational dependence produces the $\delta(eqQ)_i$ constants and deviations shown in Table IV.

C. Effect of vibration-rotation interaction

The quadrupole resonance for higher vibrational states are sometimes affected by coupling between different vibrational modes through vibration-rotation interaction. Although this interaction leaves J a good quantum number, the other quantum numbers such as K and l are mixed. The quadrupole spectrum is affected because of the variation of K which appears in the factor $3K^2/J(J+1)-1$ in Eq. (28). The vibrational angular momentum l is not "felt" by the nucleus whose orientation is space fixed and, as in the case of Stark or Zeeman Hamiltonian does not appear in the energy expression.

A good example is provided by the quadrupole resonances associated with the $^rR(20,2)$ $\nu_5 \leftarrow \nu_3$ transition, which is coincident with the N_2O $R(9)$ laser line. A straightforward analysis of the resonances corresponding to the upper state produces eqQ value of -1902.7 ± 2.2 MHz which is very different from the value -1934.5 ± 3.0 MHz for the ν_5 state previously obtained by microwave experiment.[33(b)] This is explained as due to the strong Coriolis mixing between the $|\nu_5, J, k=\pm 3,\ l=\pm 1\rangle$ state and the $|\nu_3+\nu_6, J, k=\pm 4, l=\mp 1\rangle$ state which is enhanced because of the accidental near degeneracy.[32] This mixing makes the effective K value larger than 3.

Considering also the strong Fermi interaction between the ν_5 and the $\nu_3+\nu_6$ states, we can write the wave function for the upper state as a linear combination:

$$\alpha|\nu_5, J, \pm k, l=\pm 1\rangle + \beta|\nu_3+\nu_6, J, \pm k, l=\pm 1\rangle + \gamma|\nu_5, J, \pm(k+1), l=\mp 1\rangle + \delta|\nu_3+\nu_6, J, \pm(k+1), l=\mp 1\rangle ,$$

where the coefficients α, β, γ, and δ can be derived from an analysis of Fermi and Coriolis interactions.

The quadrupole energy is then given by

$$\left[(eqQ_{\nu_5}|\alpha|^2+eqQ_{\nu_3+\nu_6}|\beta|^2)\left(\frac{3k^2}{J(J+1)}-1\right)+(eqQ_{\nu_5}|\gamma|^2+eqQ_{\nu_3+\nu_6}|\delta|^2)\left(\frac{3(k+1)^2}{J(J+1)}-1\right)\right]f(I,J,F).$$

The available values of $|\alpha|^2=0.59\pm0.08$, $|\beta|^2=0.04\pm0.02$, $|\gamma|^2=0.13\pm0.04$, and $|\delta|^2=0.24\pm0.06$ for the $|\nu_5, J=20, k=\pm3, l=\pm1\rangle$ state are not sufficiently accurate to determine the value of eqQ_{ν_5} but explain the observed frequencies satisfactorily.

D. FIR laser lines

The CH_3I molecule has been used for obtaining infrared laser emission by pumping with CO_2 lasers in the 10.4 and 9.4-μm region.[37,38] For the three observed lines reported first, Graner gave assignments using the observed FIR wavelength and rovibrational constants for the ν_6-0 and $2\nu_3-0$ bands.[39] Graner's assignments have been confirmed in the present work. In Table V we summarize all the FIR laser lines observed for CH_3I [except for the cascading transitions on the $10P(18)$ line] together with the molecular infrared transitions assigned in this work. For most lines the FIR wavelength corresponds to the $\Delta K=0$ transition in the upper state.

Although both FIR laser and the ir-rf double resonance (PQR) require near coincidences, other requirements are different and these two observations are sometimes complementary. The laser lines with which FIR but not PQR signals are observed are probably off resonant. For the FIR experiment in which higher gas pressure and higher laser power is used, the infrared pumping is realized because of pressure broadening or saturation broadening. An example is the $P(36)$ laser line at the 10.76 μm which pumps the ${}^rP(39,8)$ ν_6-0 line and gives FIR. This laser line is separated from the molecular transition by 0.017 cm^{-1} and does not produce a PQR signal. On the other hand, those laser lines which produce strong PQR signals but not FIR are resonant to relatively low J transitions. The wavelengths for rotational transitions associated with these low J transitions are too large to generate FIR efficiently.

Many new coincidences detected and assigned in this paper, listed in Table I, can be used for future FIR generations.

VII. DISCUSSION

The results described in this paper demonstrate the very high sensitivity of the method of incavity double resonance. The signal-to-noise ratio for

TABLE V. Assignment of far infrared lines of CH_3I.

λ (μm)	CO_2 pump lines	Reference	ir assignment[a]	ir coincidences in PQR[a]
377.45	9R16	37,38	${}^qR(53,3)2\nu_3-0$	Same
390.53	10P42	37,38	${}^rR(53,9)\nu_3+\nu_6-\nu_3$	Same; ${}^rQ(15,5)\nu_2+\nu_6-\nu_2$
392.48	9R14	38		None
447.17	10P18	37,38	${}^rR(44,5)\nu_6-0$	Same
459.18	10P8	38		${}^rR(9,8)\nu_6-0$
477.87	9P26	38		None
508.37	9P34	38	${}^rP(41,3)2\nu_3-0$	Same
517.33	10P14	38		None
525.32	9P4	38	${}^qR(38,5)3\nu_3-\nu_3$	Same; ${}^qR(37,2)3\nu_3-\nu_3$
529.28	10P36	38	$[{}^rP(39,8)\nu_6-0]$[b]	${}^rR(9,5)2\nu_6-\nu_6$
542.99	10P26	37,38	${}^rR(38,5)\nu_6-0\,{}^{13}CH_3I$	Same
576.17	10P16	37,38	${}^rR(34,6)2\nu_6-\nu_6$	Same
578.90	10R34	38	${}^rR(34,11)\nu_3+\nu_6-\nu_3$	Same
583.87	9P4	38		See $\lambda=525.32$ μm
639.73	9P6	38	${}^qR(31,5)3\nu_3-\nu_3$	Same
670.99	10P28	38		None
719.30	10P22	37,38		See $\lambda=964$ μm
964.0	10P22	37	${}^rQ(21,8)\nu_3+\nu_6-\nu_3$	Same
1063.29	10P38	37,38	${}^rR(18,5)\nu_3+\nu_6-\nu_3$	Same
1253.73	10P32	37,38	${}^rR(15,5)\nu_6-0$	Same

[a] ir lines of ${}^{12}CH_3I$ molecule, unless otherwise specified.
[b] Tentative assignment only.

direct double-resonance signals are often more than 10^4 at a time constant of 30 msec. Even the weaker collision-induced resonances and hot bands are observed with large signal-to-noise ratios.

Compared with the molecular beam electric resonance method, the double-resonance method has the following advantages: (i) the apparatus is simpler and less expensive to build and the method is applicable to many molecules; (ii) studies of molecules in higher rotational and vibrational states are possible; (iii) keeping molecules in the normal gaseous state enables us to study collisional effects; and (iv) many multiphoton processes involving ir and rf radiation can be studied.

The limitations of the method are as follows: (a) the molecule has to have transitions in the 9–11-μm region of the CO_2 or N_2O laser. If a CO laser is available the 7–5-μm region can also be used; (b) we have to rely on chance coincidences of a laser line and a molecular transition; and (c) the inherent requirement of infrared saturation reduces the accuracy of rf measurement through power broadening and ac Stark shift.

These considerations indicate that the method of double resonance is most useful for relatively heavy molecules for which many coincidences are expected.

The high sensitivity of this method has already been applied to the study of multiphoton processes,[2b] "forbidden" rotational transitions,[40] Λ-type doubling of NO,[41] K doubling of H_2CO and HDCO,[42] and l doubling of CD_3F.[43] It may be possible in the future to use this method for observing unstable molecular species such as free radicals, molecular ions and charge transfer complexes. The characteristic pattern of hyperfine structure may help the assignment of the spectra.

ACKNOWLEDGMENTS

J. Burie, D. Boucher, J. Demaison, and A. Dubrulle kindly sent us the computer program which was used for the analysis of hyperfine structure and also unpublished results of hyperfine constants for the ground state determined from their molecular-beam experiments. J. Sakai sent us his results of "pure" quadrupole resonances prior to publication. A. E. Douglas, G. Herzberg, H. Lew, and A. R. W. McKellar read this paper and gave us critical comments. To all of them we are grateful.

---

*Permanent address: Istituto di Fisica dell' Universita', Piazza Torricelli 2, 56100 Pisa, Italy.

†Permanent address: Laboratorie de Spectroscopie Hertzienne, Université des Sciences et Techniques de Lille, BP36, 59650, Villeneuve-d'Ascq, France.

[1]Preliminary results of this paper have been published in (a) Proceedings of Meeting of Division of Atomic and Molecular Physics of Canadian Association of Physicists, Ottawa, 1976; (b) Abstracts of Symposium on Molecular Structure and Spectroscopy, Columbus, Ohio, 1977; and (c) *Laser Spectroscopy III*, edited by J. L. Hall and J. L. Carlsten (Springer-Verlag, New York, 1977).

[2]For a summary see (a) K. Shimoda, *Laser Spectroscopy of Atoms and Molecules, Topics in Applied Physics*, Vol. 2, edited by H. Walther, (Springer-Verlag, New York, 1976, p. 197, or (b) T. Oka, *Frontiers in Laser Spectroscopy*, Les Houches Summer School Proceedings Session XXVII, edited by R. Balian, S. Haroche, and S. Liberman (North-Holland, Amsterdam, 1977).

[3]T. P. Das and E. L. Hahn, *Nuclear Quadrupole Resonance Spectroscopy* (Academic, New York, 1958).

[4]F. Sterzer and Y. Beers, Phys. Rev. 100, 1174 (1955).

[5]N. G. Basov and B. D. Osipov, Opt. Spektrosk., 4, 795 (1954).

[6]B. D. Osipov, Opt. Spektrosk. 8, 581 (1960) [Opt. Spectrosc. 8, 309 (1960)].

[7]K. Shimoda, J. Phys. Soc. Jpn. 14, 954 (1959).

[8]J. Sakai, Proceedings of the Meeting on Molecular Structure, Tokyo, 1976; *ibid.*, Sapporo, 1977.

[9]M. Takami and K. Shimoda, Jpn. J. Appl. Phys. 11, 1648 (1972); M. Takami, *ibid.* 15, 1063 (1976); 15, 1889 (1976).

[10]R. F. Wormsbecher, D. O. Harris, and B. G. Wicke, J. Mol. Spectrosc. 64, 86 (1977).

[11]J. W. C. Johns, A. R. W. McKellar, T. Oka, and M. Römheld, J. Chem. Phys. 62, 1488 (1975).

[12]M. Sargent, III, M. O. Scully, and W. E. Lamb, Jr., *Laser Physics* (Addison-Wesley, Reading, Mass., 1974).

[13]S. M. Freund and T. Oka, Phys. Rev. A 13, 2178 (1976).

[14]W. A. Kreiner and T. Oka, Can. J. Phys. 53, 2000 (1975).

[15]T. Oka, Adv. At. Mol. Phys. 9, 127 (1973).

[16]M. Ouhayoun and C. Bordé, C. R. Acad. Sci. B 274, 411 (1972).

[17]T. W. Meyer and C. K. Rhodes, Phys. Rev. Lett. 32, 637 (1974); W. K. Bischel and C. K. Rhodes, Phys. Rev. A 14, 176 (1976).

[18]R. G. Brewer, R. L. Shoemaker, and S. Stenholm, Phys. Rev. Lett. 33, 63 (1974); R. L. Shoemaker, S. Stenholm, and R. G. Brewer, Phys. Rev. A 10, 2037, (1974).

[19]S. M. Freund, J. W. C. Johns, A. R. W. McKellar, and T. Oka, J. Chem. Phys. 59, 3445 (1973).

[20]M. Takami and K. Shimoda, Jpn. J. Appl. Phys. 12, 934 (1973).

[21]T. K. Hänsch, A. L. Schawlow, and P. E. Toschek, IEEE J. Quantum Electron. QE-8, 802 (1972).

W. Brunner and H. Paul, Opt. Commun. 12, 252 (1974).
[22]H. V. Holt, Phys. Rev. 11, 625 (1975); 14, 1901 (1976).
[23]A. N. Rubinov and M. V. Belokon', Sov. J. Quantum Electron. 6, 79 (1976).
[24]C. H. Townes and A. L. Schawlow, *Microwave Spectroscopy* (McGraw-Hill, New York, 1955).
[25]J. T. Hougen, J. Chem. Phys. 57, 4207 (1972).
[26]J. Burie, D. Boucher, J. Demaison, and A. Dubrulle, Mol. Phys. 32, 289 (1976).
[27]W. A. Kreiner, V. Andresen, and T. Oka, J. Chem. Phys. 66, 4662 (1977).
[28]H. Matsumura and J. Overend, Spectrochim. Acta. A 27, 2165 (1971).
[29]E. W. Jones and H. W. Thompson, Proc. R. Soc. A 288, 50 (1965).
[30]J. B. Cohen and E. B. Wilson, J. Chem. Phys. 58, 456 (1973).
[31]W. A. Kreiner, A. Eyer, and H. Jones, J. Mol. Spectrosc. 52, 420 (1974).
[32]H. Matsumura, T. Nakagawa, and J. Overend, J. Chem. Phys. 59, 1449 (1973).
[33](a) Y. Morino and C. Hirose, J. Mol. Spectrosc. 22, 99 (1967). (b) Y. Kawashima and C. Hirose, Bull. Chem. Soc. Jpn. 46, 2969 (1975).
[34]J. L. Duncan and A. Allan, Spectrochim. Acta A 25, 901 (1969). There is a miscalculation in this paper. The band origin $\nu_6 \leftarrow 0$ should read 881.90 cm^{-1} and $[(A'-A'') - (B'-B'')] = 0.0342\ cm^{-1}$.
[35]J. L. Hall and J. A. Magyar, in *Topics in Applied Physics*, Vol. 13, edited by K. Shimoda (Springer-Verlag, Berlin, 1976), p. 173.
[36]J. Burie (private communication).
[37]S. F. Dyubko, L. D. Fesenko, O. I. Baskakov, and V. A. Svich, Zh. Prikl, Spektrosk. 23. 317 (1975).
[38]T. Y. Chang and J. D. McGee, IEEE J. Quantum Electron. QE-1, 62 (1976).
[39]G. Graner, Opt. Commun. 14, 67 (1975).
[40]For a summary, see, T. Oka, *Molecular Spectroscopy: Modern Research*, Vol. II, edited by K. Narahari Rao, (Academic, New York, 1976), p. 229.
[41]R. M. Dale, J. W. C. Johns, A. R. W. McKellar, and M. Riggin, J. Mol. Spectrosc. 67, 440 (1977).
[42]P. Glorieux and G. W. Hills, J. Mol. Spectrosc. (to be published).
[43]G. Duxbury and S. M. Freund, J. Mol. Spectrosc. 67, 219 (1977).